Fluid Dynamics Research

The Japan Society of Fluid Mechanics

PAPER

Effects of the vessel bottom wall on a particle rising in an electrically conducting fluid under a strong vertical magnetic field

IOP Publishing | The Japan Society of Fluid Mechanics Fluid *Dynamics* Research

Fluid Dyn. Res. **51** (2019) 025501 (17pp) https://doi.org/10.1088/1873-7005/aaf835

Effects of the vessel bottom wall on a particle rising in an electrically conducting fluid under a strong vertical magnetic field

Kazuyuki Ueno[1], **Sachi Harada**[1] **and Masahide Watabe**[2]

[1] Department of Mechanical Engineering, Iwate University, Morioka 020-8551, Japan
[2] Department of Aerospace Engineering, Tohoku University, Sendai 980-8579, Japan

E-mail: uenok@iwate-u.ac.jp

Received 23 April 2018, revised 28 August 2018
Accepted for publication 12 December 2018
Published 29 January 2019

Communicated by Yasuhide Fukumoto

Abstract

The drag of a particle rising along a vertical magnetic field in an electrically conducting fluid is studied when the vessel bottom wall exists. A dynamically similar flow using compressed coordinates is obtained when the Hartmann number is much greater than one, the Reynolds number is much smaller than the Hartmann number, and the magnetic Reynolds number is much smaller than one. The drag influenced by the vessel bottom wall is derived from this similar solution. A correction term with respect to the vessel bottom wall is added to Chester's drag in free space. The drag of the particle increases when the distance between the particle and vessel bottom wall decreases. The region of influence of the vessel bottom wall spreads along the magnetic flux lines when the Hartmann number increases. Therefore, the correction term of drag affects a large region in the vessel when the magnetic field is very strong.

Keywords: magnetohydrodynamics, drag, Hartmann number, vessel bottom wall

1. Introduction

The drag of a small particle with radius a is given by Stokes's drag law:

$$D_{\text{stokes}} = 6\pi\eta a U_0, \tag{1}$$

when it moves at velocity U_0 in a viscous fluid with viscosity η. This prediction is valid when the Reynolds number based on particle size is much smaller than one. Stokes's drag (1) and its various extensions are utilized in many fields of study.

According to Chester's study (Chester 1961, Chester and Moore 1961), the drag of a particle which rises or falls in electrically conducting fluid under strong vertical magnetic field is given by

$$D_{\text{chester}} = 2\pi(\sigma\eta)^{1/2}a^2U_0B_0 = 2\pi\eta aU_0Ha, \tag{2}$$

where σ and B_0 denote the electric conductivity and magnetic flux density, respectively, and the Hartmann number is as follows:

$$Ha = (\sigma/\eta)^{1/2}aB_0. \tag{3}$$

Prediction (2) is valid when Hartmann number Ha is much greater than one, and the Reynolds number based on particle size is much smaller than one. The drag increases in proportion to the magnetic flux density.

Chester's drag (2) was obtained in the 1960s. However, Chester's drag did not receive much attention in those days because it was difficult to generate a strong magnetic field that satisfies the applicable condition for Chester's drag. In recent years, the experiments satisfying the applicable condition for Chester's drag were realized via the development of the superconducting magnet. For example, Yasuda *et al* (2001, 2003) reported that the gravity segregation of monotectic alloy is suppressed when it solidifies under a strong magnetic field at 10 T. Monotectic alloys exhibit the behavior of separation into a liquid–liquid two-phase state. Therefore, gravity segregation occurs owing to the density difference in the absence of the magnetic field. Cooling the monotectic alloy under a strong magnetic field suppresses gravity segregation because the drag of the droplet increases and the rising velocity or falling velocity of the droplet decreases.

The studies of Chang (1963), Kyrlidis *et al* (1990), and Ueno and Yasuda (2003) demonstrate that single spheres rise or fall in an electrically conducting fluid in free space under a strong vertical magnetic field. These studies elucidated that the flow field has strong anisotropy in the direction parallel to the magnetic field. The magnetic field influences over distance in the direction of the magnetic field.

In many problems related to electrically conducting fluid flows, the fluid is confined in a vessel. The drag of a particle rising in the fluid in a vessel differs from that in free space. However, to the best of our knowledge, the vessel wall has not been taken into account in any study.

This paper describes the effect of the vessel bottom wall on the rising particle. We consider the rising particle as a solid sphere. The result of this study is applicable to droplets, bubbles, and spheroids. We consider the particle as a rising body; however, the result can be applied to falling particles by changing the sign of the field functions. We consider a semi-infinite problem with respect to the vessel bottom wall, while vessel walls that are parallel to the magnetic field are not considered.

2. Compressed coordinates and simplified equations

We consider a rising particle in an electrically conducting fluid in a superconducting magnet, as shown in figure 1. The magnetic flux density induced by the magnet is idealized as $\boldsymbol{B} = B_0\,\boldsymbol{e}_z$, where B_0 is a given constant, and $\boldsymbol{e}_z$ is the unit vector in vertical direction z. We discuss the flow fields when the magnetic Reynolds number is much smaller than one. Thus, the magnetic field induced by the current in the conductive fluid is negligibly small. Furthermore, we assume that the z-component of current density, z-component of vorticity, and scalar potential of electric field are always 0. These assumptions have no contradiction when the particle rises parallel to the z-axis. Under these assumptions, the Ohm's law is

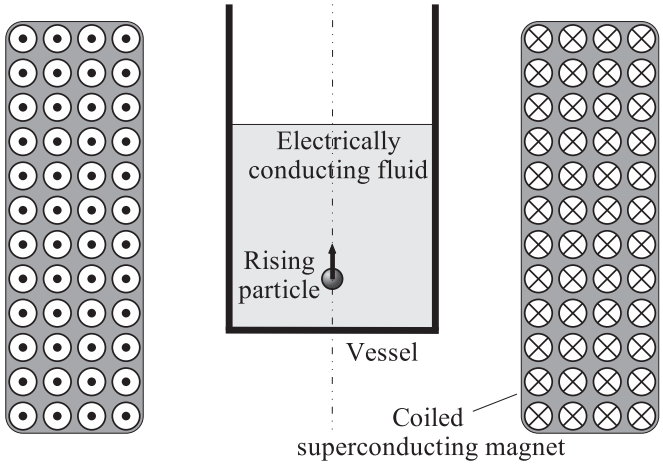

Figure 1. A particle rising in electrically conducting fluid under strong vertical magnetic field.

reduced to

$$j_x = \sigma u_y B_0, \qquad j_y = -\sigma u_x B_0, \qquad j_z = 0, \tag{4}$$

where $\boldsymbol{u} = u_x \boldsymbol{e}_x + u_y \boldsymbol{e}_y + u_z \boldsymbol{e}_z$ denotes velocity, and $\boldsymbol{j} = j_x \boldsymbol{e}_x + j_y \boldsymbol{e}_y$ denotes current density. The constant σ is the electric conductivity of the fluid, and $\boldsymbol{e}_x$ and $\boldsymbol{e}_y$ denote the unit vectors parallel to the x-axis and y-axis, respectively. Taking the above relation into account, the Lorentz force acting on the fluid is given by $\boldsymbol{j} \times \boldsymbol{B} = -\sigma {B_0}^2 (u_x \boldsymbol{e}_x + u_y \boldsymbol{e}_y)$.

Let us introduce the following dimensionless variables:

$$\begin{aligned} &x = a\tilde{x}, \quad y = a\tilde{y}, \quad z = a\tilde{z}, \quad t = (a/U_0)\tilde{t}, \\ &u_x = U_0 \tilde{u}_x, \quad u_y = U_0 \tilde{u}_y, \quad u_z = U_0 \tilde{u}_z, \\ &p = p_0 - \rho g z + \sigma a {B_0}^2 U_0 \tilde{p}, \end{aligned} \tag{5}$$

where a denotes the radius of a particle, and $\tilde{x}$, $\tilde{y}$, and $\tilde{z}$ are dimensionless coordinates. The rising velocity of the particle is denoted by U_0, and $\tilde{u}_x \boldsymbol{e}_x + \tilde{u}_y \boldsymbol{e}_y + \tilde{u}_z \boldsymbol{e}_z$ is the dimensionless flow velocity. Constants p_0, ρ, and g denote representative values of pressure, fluid density, and gravitational acceleration, respectively. The variables $\tilde{t}$ and $\tilde{p}$ denote the dimensionless time and dimensionless pressure, respectively. The governing equations of the present problem in dimensionless form are given as follows:

$$\frac{\partial \tilde{u}_x}{\partial \tilde{x}} + \frac{\partial \tilde{u}_y}{\partial \tilde{y}} + \frac{\partial \tilde{u}_z}{\partial \tilde{z}} = 0, \tag{6}$$

$$\begin{aligned} &\frac{Re}{Ha^2}\left(\frac{\partial \tilde{u}_x}{\partial \tilde{t}} + \tilde{u}_x \frac{\partial \tilde{u}_x}{\partial \tilde{x}} + \tilde{u}_y \frac{\partial \tilde{u}_x}{\partial \tilde{y}} + \tilde{u}_z \frac{\partial \tilde{u}_x}{\partial \tilde{z}} \right) \\ &\quad = -\frac{\partial \tilde{p}}{\partial \tilde{x}} + \frac{1}{Ha^2}\left(\frac{\partial^2 \tilde{u}_x}{\partial \tilde{x}^2} + \frac{\partial^2 \tilde{u}_x}{\partial \tilde{y}^2} + \frac{\partial^2 \tilde{u}_x}{\partial \tilde{z}^2} \right) - \tilde{u}_x, \end{aligned} \tag{7}$$

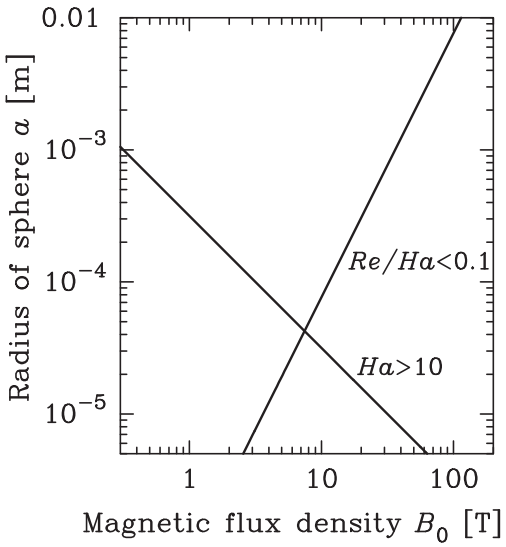

Figure 2. B_0–a diagram of a copper droplet rising in molten lead at 950 °C.

$$\frac{Re}{Ha^2}\left(\frac{\partial \tilde{u}_y}{\partial \tilde{t}} + \tilde{u}_x\frac{\partial \tilde{u}_y}{\partial \tilde{x}} + \tilde{u}_y\frac{\partial \tilde{u}_y}{\partial \tilde{y}} + \tilde{u}_z\frac{\partial \tilde{u}_y}{\partial \tilde{z}}\right) = -\frac{\partial \tilde{p}}{\partial \tilde{y}} + \frac{1}{Ha^2}\left(\frac{\partial^2 \tilde{u}_y}{\partial \tilde{x}^2} + \frac{\partial^2 \tilde{u}_y}{\partial \tilde{y}^2} + \frac{\partial^2 \tilde{u}_y}{\partial \tilde{z}^2}\right) - \tilde{u}_y, \tag{8}$$

$$\frac{Re}{Ha^2}\left(\frac{\partial \tilde{u}_z}{\partial \tilde{t}} + \tilde{u}_x\frac{\partial \tilde{u}_z}{\partial \tilde{x}} + \tilde{u}_y\frac{\partial \tilde{u}_z}{\partial \tilde{y}} + \tilde{u}_z\frac{\partial \tilde{u}_z}{\partial \tilde{z}}\right) = -\frac{\partial \tilde{p}}{\partial \tilde{z}} + \frac{1}{Ha^2}\left(\frac{\partial^2 \tilde{u}_z}{\partial \tilde{x}^2} + \frac{\partial^2 \tilde{u}_z}{\partial \tilde{y}^2} + \frac{\partial^2 \tilde{u}_z}{\partial \tilde{z}^2}\right). \tag{9}$$

It is noteworthy that the driving force of the rising particle is the pressure difference between the upper surface and the lower surface of the particle (buoyancy force), included in (5), though the gravitational force in the negative z direction does not appear in the above dimensionless equations.

The boundary conditions in the dimensionless form are as follows:

$$\begin{aligned} &\tilde{\boldsymbol{u}} = \boldsymbol{e}_z && \text{at} \quad \tilde{x}^2 + \tilde{y}^2 + (\tilde{z} - \tilde{l}\ )^2 = 1, \\ &\tilde{\boldsymbol{u}} = \boldsymbol{0} && \text{at} \quad \tilde{z} = 0, \\ &\tilde{\boldsymbol{u}} \to \boldsymbol{0} && \text{for} \quad \tilde{x}^2 + \tilde{y}^2 \to \infty, \end{aligned} \tag{10}$$

where the origin of the coordinates is located on the bottom wall. Parameter $\tilde{l} = l/a$ denotes the distance between the center of the particle and the bottom wall. The effect of the side walls is not taken into account in the present study. The validity of this assumption is demonstrated by the results. The effect of a top wall or upper free surface is also not taken into account. The conductivity of the bottom wall does not affect the particle because there are no electric field and no z-component of current density.

In the following part of this paper, we consider the flow for $Ha \gg 1$ and $Re \ll Ha$. Figure 2 shows B_0–a diagram of a copper droplet rising in molten lead at 950 °C. This

diagram is divided into four domains by $Ha = 10$ and $ReHa^{-1} = 0.1$, where the properties of molten lead are as follows: $\sigma = 1 \times 10^6\,\mathrm{S\,m^{-1}}$, $\eta = 1 \times 10^{-3}\,\mathrm{Pa\,s}$, $\rho_{\mathrm{Pb}} = 10 \times 10^3\,\mathrm{kg\,m^{-3}}$ and $\rho_{\mathrm{Pb}} - \rho_{\mathrm{Cu}} = 2 \times 10^3\,\mathrm{kg\,m^{-3}}$. The rising velocity U_0 is determined so as to balance the drag with buoyancy $\frac{4}{3}\pi a^3(\rho_{\mathrm{Pb}} - \rho_{\mathrm{Cu}})g$ of the particle. Drag is tentatively estimated by Chester's drag law (2):

$$U_0 = \frac{2a(\rho_{\mathrm{Pb}} - \rho_{\mathrm{Cu}})g}{3(\sigma\eta)^{1/2}B_0}. \tag{11}$$

This U_0 gives $Re = \rho_{\mathrm{Pb}}U_0\,a/\eta = 2a^2\rho_{\mathrm{Pb}}(\rho_{\mathrm{Pb}} - \rho_{\mathrm{Cu}})g/(3\sigma^{1/2}\eta^{3/2}B_0)$ and $Re/Ha = 2a\rho_{\mathrm{Pb}}(\rho_{\mathrm{Pb}} - \rho_{\mathrm{Cu}})g/(3\sigma\eta B_0{}^2)$. For a magnetic flux density of 10 T, particles of $4 \times 10^{-5} < a < 8 \times 10^{-5}$ m satisfy the conditions $Ha > 10$ and $Re/Ha < 0.1$.

In order to obtain an asymptotic solution of (7)–(9) for $Ha^{-1} \ll 1$ and $ReHa^{-1} \ll 1$, we compress the coordinate $\tilde{z}$ as follows:

$$\begin{gathered}\tilde{x} = \hat{x}, \quad \tilde{y} = \hat{y}, \quad \tilde{z} = Ha\hat{z}, \quad \tilde{t} = Ha\hat{t}, \\ \tilde{u}_x = Ha^{-1}\hat{u}_x, \quad \tilde{u}_y = Ha^{-1}\hat{u}_y, \quad \tilde{u}_z = \hat{u}_z, \quad \tilde{p} = Ha^{-1}\hat{p}.\end{gathered} \tag{12}$$

The governing equations expressed in compressed coordinate are as follows:

$$\frac{\partial \hat{u}_x}{\partial \hat{x}} + \frac{\partial \hat{u}_y}{\partial \hat{y}} + \frac{\partial \hat{u}_z}{\partial \hat{z}} = 0, \tag{13}$$

$$\begin{aligned}&\frac{Re}{Ha^3}\left(\frac{\partial \hat{u}_x}{\partial \hat{t}} + \hat{u}_x\frac{\partial \hat{u}_x}{\partial \hat{x}} + \hat{u}_y\frac{\partial \hat{u}_x}{\partial \hat{y}} + \hat{u}_z\frac{\partial \hat{u}_x}{\partial \hat{z}}\right) \\ &\quad = -\frac{\partial \hat{p}}{\partial \hat{x}} + \frac{1}{Ha^2}\left(\frac{\partial^2 \hat{u}_x}{\partial \hat{x}^2} + \frac{\partial^2 \hat{u}_x}{\partial \hat{y}^2} + \frac{1}{Ha^2}\frac{\partial^2 \hat{u}_x}{\partial \hat{z}^2}\right) - \hat{u}_x,\end{aligned} \tag{14}$$

$$\begin{aligned}&\frac{Re}{Ha^3}\left(\frac{\partial \hat{u}_y}{\partial \hat{t}} + \hat{u}_x\frac{\partial \hat{u}_y}{\partial \hat{x}} + \hat{u}_y\frac{\partial \hat{u}_y}{\partial \hat{y}} + \hat{u}_z\frac{\partial \hat{u}_y}{\partial \hat{z}}\right) \\ &\quad = -\frac{\partial \hat{p}}{\partial \hat{y}} + \frac{1}{Ha^2}\left(\frac{\partial^2 \hat{u}_y}{\partial \hat{x}^2} + \frac{\partial^2 \hat{u}_y}{\partial \hat{y}^2} + \frac{1}{Ha^2}\frac{\partial^2 \hat{u}_y}{\partial \hat{z}^2}\right) - \hat{u}_y,\end{aligned} \tag{15}$$

$$\begin{aligned}&\frac{Re}{Ha}\left(\frac{\partial \hat{u}_z}{\partial \hat{t}} + \hat{u}_x\frac{\partial \hat{u}_z}{\partial \hat{x}} + \hat{u}_y\frac{\partial \hat{u}_z}{\partial \hat{y}} + \hat{u}_z\frac{\partial \hat{u}_z}{\partial \hat{z}}\right) \\ &\quad = -\frac{\partial \hat{p}}{\partial \hat{z}} + \left(\frac{\partial^2 \hat{u}_z}{\partial \hat{x}^2} + \frac{\partial^2 \hat{u}_z}{\partial \hat{y}^2} + \frac{1}{Ha^2}\frac{\partial^2 \hat{u}_z}{\partial \hat{z}^2}\right).\end{aligned} \tag{16}$$

By neglecting the small terms $\mathrm{O}(Ha^{-2})$ and $\mathrm{O}(ReHa^{-1})$ after the coordinate compression, we obtain the following simplified equations:

$$\frac{\partial \hat{u}_x}{\partial \hat{x}} + \frac{\partial \hat{u}_y}{\partial \hat{y}} + \frac{\partial \hat{u}_z}{\partial \hat{z}} = 0, \tag{17}$$

$$-\frac{\partial \hat{p}}{\partial \hat{x}} - \hat{u}_x = 0, \tag{18}$$

$$-\frac{\partial \hat{p}}{\partial \hat{y}} - \hat{u}_y = 0, \tag{19}$$

$$-\frac{\partial \hat{p}}{\partial \hat{z}} + \frac{\partial^2 \hat{u}_z}{\partial \hat{x}^2} + \frac{\partial^2 \hat{u}_z}{\partial \hat{y}^2} = 0. \tag{20}$$

Inertia terms are neglected like Stokes approximation for non-conducting fluids. Furthermore, viscous terms are neglected in (18), (19) and $\partial^2 \hat{u}_z/\partial \hat{z}^2$ is neglected in (20) owing to the anisotropy of conducting fluids along magnetic field. Consequently, equations (17)–(20) are reduced to a system of spatially-developing parabolic equations as mentioned later. They have properties similar to Oseen approximation for non-conducting fluids (Ueno and Yasuda 2003) rather than Stokes approximation.

The boundary conditions in the compressed coordinates are given as follows:

$$\begin{aligned} &\hat{u}_z = 1 \qquad \text{at} \quad \hat{z} = \hat{l} \pm 0, \quad 0 \leqslant \hat{x}^2 + \hat{y}^2 \leqslant 1, \\ &\hat{u}_z = 0 \qquad \text{at} \quad \hat{z} = 0, \\ &\hat{\boldsymbol{u}} \to \boldsymbol{0} \qquad \text{for} \quad \hat{x}^2 + \hat{y}^2 \to \infty. \end{aligned} \tag{21}$$

The particle is reduced to a disk in the compressed coordinates. The upper surface and the lower surface of the rising particle (or disk) are denoted as $\hat{z} = \hat{l} + 0$ and $\hat{z} = \hat{l} - 0$, respectively.

Simplified equations (17)–(21) contain only one parameter $\hat{l} = l/(a\,Ha)$; i.e. the flow fields for $Ha^{-1} \ll 1$ and $ReHa^{-1} \ll 1$ are in dynamical similarity characterized by $\hat{l}$. The anisotropy of the flow field is included not in the similar solution but in the coordinate compression.

3. Spatial-evolution functions

Equations (17)–(20) are reduced as follows:

$$\left\{\left(\frac{\partial^2}{\partial \hat{x}^2} + \frac{\partial^2}{\partial \hat{y}^2}\right)^2 - \frac{\partial^2}{\partial \hat{z}^2}\right\}\hat{u}_z = 0, \tag{22}$$

$$\left\{\left(\frac{\partial^2}{\partial \hat{x}^2} + \frac{\partial^2}{\partial \hat{y}^2}\right)^2 - \frac{\partial^2}{\partial \hat{z}^2}\right\}\hat{p} = 0. \tag{23}$$

In order to obtain solutions of the 4th order equations (22) and (23), we introduce functions $\hat{f}_{\mathrm{up}}$, $\hat{f}_{\mathrm{down}}$ satisfying the following 2nd order parabolic equations.

$$\left\{\left(\frac{\partial^2}{\partial \hat{x}^2} + \frac{\partial^2}{\partial \hat{y}^2}\right) - \frac{\partial}{\partial \hat{z}}\right\}\hat{f}_{\mathrm{up}} = 0, \tag{24}$$

$$\left\{\left(\frac{\partial^2}{\partial \hat{x}^2} + \frac{\partial^2}{\partial \hat{y}^2}\right) + \frac{\partial}{\partial \hat{z}}\right\}\hat{f}_{\mathrm{down}} = 0. \tag{25}$$

The function $\hat{f}_{\mathrm{up}}$ spatially develops from the lower boundary in the positive $\hat{z}$ direction, while $\hat{f}_{\mathrm{down}}$ spatially develops from the upper boundary in the negative $\hat{z}$ direction.

Velocity $\hat{u}_z$ and pressure $\hat{p}$ are obtained by the following sums of $\hat{f}_{\mathrm{up}}$ and $\hat{f}_{\mathrm{down}}$.

$$\hat{u}_z = C_1 \hat{f}_{\mathrm{up}} + C_2 \hat{f}_{\mathrm{down}} + C_3, \tag{26}$$

$$\hat{p} = C_4\hat{f}_{\rm up} + C_5\hat{f}_{\rm down} + C_6, \tag{27}$$

where $C_1, C_2, \cdots, C_6$ denote constants. These functions automatically satisfy (22), (23). Since $\hat{u}_z$ and $\hat{p}$ are not independent, the constants $C_1, C_2, \cdots, C_6$ are also not independent. Substituting (26), (27) into (17)–(20), we obtain $C_4 = C_1$, $C_5 = -C_2$. Further, $C_1\hat{f}_{\rm up} + (C_3 + C_6)/2$ and $C_2\hat{f}_{\rm down} + (C_3 - C_6)/2$ are rewritten as $\hat{f}_{\rm up}$ and $\hat{f}_{\rm down}$, respectively, and we obtain the following relations:

$$\hat{u}_z = \hat{f}_{\rm up} + \hat{f}_{\rm down}, \tag{28}$$

$$\hat{p} = \hat{f}_{\rm up} - \hat{f}_{\rm down}. \tag{29}$$

By using $\hat{f}_{\rm up}$ and $\hat{f}_{\rm down}$, boundary condition (21) is reduced as follows:

$$\begin{aligned} &\hat{f}_{\rm up} + \hat{f}_{\rm down} = 1 && \text{at} \quad \hat{z} = \hat{l} \pm 0, \quad 0 \leqslant \hat{x}^2 + \hat{y}^2 \leqslant 1, \\ &\hat{f}_{\rm up} + \hat{f}_{\rm down} = 0 && \text{at} \quad \hat{z} = 0, \\ &\hat{f}_{\rm up} \to 0, \quad \hat{f}_{\rm down} \to 0 && \text{for} \quad \hat{x}^2 + \hat{y}^2 \to \infty. \end{aligned} \tag{30}$$

Here, we consider $\hat{p} \to 0$ for $\hat{x}^2 + \hat{y}^2 \to \infty$ in the 3rd line of (30).

If we obtain the solutions of $\hat{f}_{\rm up}, \hat{f}_{\rm down}$ satisfying (24), (25), and (30), the velocity $\hat{u}_z$ and the pressure $\hat{p}$ are given by (28) and (29). Furthermore, taking (18) and (19) into account, $\hat{u}_x$, $\hat{u}_y$ are given as follows:

$$\hat{u}_x = -\frac{\partial \hat{f}_{\rm up}}{\partial \hat{x}} + \frac{\partial \hat{f}_{\rm down}}{\partial \hat{x}}, \qquad \hat{u}_y = -\frac{\partial \hat{f}_{\rm up}}{\partial \hat{y}} + \frac{\partial \hat{f}_{\rm down}}{\partial \hat{y}}. \tag{31}$$

4. Formulation by the Green function method

4.1. Convolution integral of the boundary value

Let us introduce the following free-space Green function for (24):

$$\hat{G}_{\rm up} = \begin{cases} \dfrac{1}{4\pi(\hat{z} - \hat{\zeta})} \exp\left(-\dfrac{(\hat{x} - \hat{\xi})^2 + (\hat{y} - \hat{\eta})^2}{4(\hat{z} - \hat{\zeta})} \right) & \text{for } \hat{z} \geqslant \hat{\zeta}, \\ 0 & \text{for } \hat{z} < \hat{\zeta}. \end{cases} \tag{32}$$

This is the same form as the solution of the two-dimensional heat equation (Wrobel 2002) though the time t is replaced by the coordinate $\hat{z}$ parallel to the magnetic field.

Equation (24) is a homogeneous equation, and hence, the solution is given by the following convolution integral of the boundary value at $\hat{z} = \hat{\zeta}_{\rm btm}$:

$$\hat{f}_{\rm up}(\hat{x}, \hat{y}, \hat{z}) = \iint \hat{G}_{\rm up}(\hat{x}, \hat{y}, \hat{z}; \hat{\xi}, \hat{\eta}, \hat{\zeta}_{\rm btm})\, \hat{f}_{\rm up}(\hat{\xi}, \hat{\eta}, \hat{\zeta}_{\rm btm})\, {\rm d}\hat{\xi}\, {\rm d}\hat{\eta} \quad \text{for } \hat{z} > \hat{\zeta}_{\rm btm}. \tag{33}$$

Likewise, free-space Green function for (25) is introduced as follows:

$$\hat{G}_{\mathrm{down}} = \begin{cases} 0 & \text{for } \hat{z} > \hat{\zeta}, \\ -\dfrac{1}{4\pi(\hat{z}-\hat{\zeta})} \exp\left(\dfrac{(\hat{x}-\hat{\xi})^2 + (\hat{y}-\hat{\eta})^2}{4(\hat{z}-\hat{\zeta})}\right) & \text{for } \hat{z} \leqslant \hat{\zeta}, \end{cases} \tag{34}$$

and the solution of (25) is given by the following convolution integral of the boundary value at $\hat{z} = \hat{\zeta}_{\mathrm{top}}$:

$$\hat{f}_{\mathrm{down}}(\hat{x}, \hat{y}, \hat{z}) = \iint \hat{G}_{\mathrm{down}}(\hat{x}, \hat{y}, \hat{z}; \hat{\xi}, \hat{\eta}, \hat{\zeta}_{\mathrm{top}})\, \hat{f}_{\mathrm{down}}(\hat{\xi}, \hat{\eta}, \hat{\zeta}_{\mathrm{top}})\, \mathrm{d}\hat{\xi}\, \mathrm{d}\hat{\eta} \quad \text{for } \hat{z} < \hat{\zeta}_{\mathrm{top}}. \tag{35}$$

In the case of the axisymmetric problem, the above solutions are reduced to

$$\hat{f}_{\mathrm{up}}(\hat{r}, \hat{z}) = \frac{1}{2(\hat{z}-\hat{\zeta}_{\mathrm{btm}})} \int I_0\left(\frac{\hat{r}\hat{\rho}}{2(\hat{z}-\hat{\zeta}_{\mathrm{btm}})}\right) \exp\left(-\frac{\hat{r}^2+\hat{\rho}^2}{4(\hat{z}-\hat{\zeta}_{\mathrm{btm}})}\right) \hat{f}_{\mathrm{up}}(\hat{\rho}, \hat{\zeta}_{\mathrm{btm}})\hat{\rho}\, \mathrm{d}\hat{\rho} \quad \text{for } \hat{z} > \hat{\zeta}_{\mathrm{btm}}, \tag{36}$$

$$\hat{f}_{\mathrm{down}}(\hat{r}, \hat{z}) = -\frac{1}{2(\hat{z}-\hat{\zeta}_{\mathrm{top}})} \int I_0\left(-\frac{\hat{r}\hat{\rho}}{2(\hat{z}-\hat{\zeta}_{\mathrm{top}})}\right) \exp\left(\frac{\hat{r}^2+\hat{\rho}^2}{4(\hat{z}-\hat{\zeta}_{\mathrm{top}})}\right) \hat{f}_{\mathrm{down}}(\hat{\rho}, \hat{\zeta}_{\mathrm{top}})\hat{\rho}\, \mathrm{d}\hat{\rho} \quad \text{for } \hat{z} < \hat{\zeta}_{\mathrm{top}}, \tag{37}$$

where I_0 is the zeroth-order modified Bessel function.

4.2. Verification of the formulas with the modified Bessel function

Verification of formulas (36) and (37) is illustrated by the free-space problem, which has been elucidated in past studies (Chester 1961, Chester and Moore 1961, Chang 1963, Kyrlidis *et al* 1990, Ueno and Yasuda 2003).

Free space is divided to two half-spaces as shown in figure 3. The half space in $\hat{z} > \hat{l}$ is called 'domain 1,' and the other in $\hat{z} < \hat{l}$ is called 'domain 2.' The particle is shown in figure 3 in the physical space before the coordinate compression, but it is regarded as a disk during the analysis using the compressed coordinates $\hat{x}\hat{y}\hat{z}$.

In domain 1, there is no information from the upper infinite far distance. Therefore, we obtain the following trivial solution:

$$\hat{f}_{\mathrm{down}}(\hat{r}, \hat{z}) = 0 \qquad \text{in domain 1}(\hat{z} \geqslant \hat{l}). \tag{38}$$

Likewise, there is no information from the lower infinite far distance in domain 2. Therefore, we also obtain the following trivial solution:

$$\hat{f}_{\mathrm{up}}(\hat{r}, \hat{z}) = 0 \qquad \text{in domain 2}(\hat{z} \leqslant \hat{l}). \tag{39}$$

Considering trivial solutions (38) and (39), we have the lower boundary value of domain 1 as follows

$$\hat{f}_{\mathrm{up}}(\hat{r}, \hat{l}+0) = \begin{cases} 1 & \text{for } 0 \leqslant \hat{r} \leqslant 1, \\ 0 & \text{for } \hat{r} > 1, \end{cases} \tag{40}$$

where the value for $0 \leqslant \hat{r} \leqslant 1$ is obtained from the first boundary condition of (30), and the value for $\hat{r} > 1$ is obtained by continuous matching with domain 2. Substituting this boundary value at $\hat{\zeta}_{\mathrm{btm}} = \hat{l} + 0$ into (36), we obtain the following:

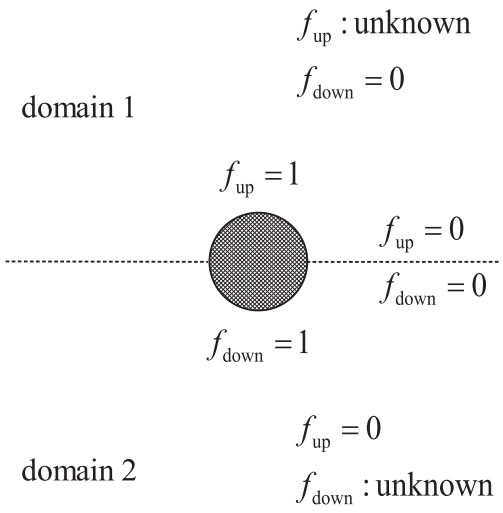

Figure 3. Division of space in the case of the free-space problem.

$$\hat{f}_{\mathrm{up}}(\hat{r},\,\hat{z}) = \frac{1}{2(\hat{z}-\hat{l})}\int_0^1 I_0\left(\frac{\hat{r}\hat{\rho}}{2(\hat{z}-\hat{l})}\right)\exp\left(-\frac{\hat{r}^2+\hat{\rho}^2}{4(\hat{z}-\hat{l})}\right)\hat{\rho}\;\mathrm{d}\hat{\rho}$$
$$\text{in domain } 1(\hat{z} > \hat{l}). \tag{41}$$

Likewise, the following value at the upper boundary of domain 2 is obtained from the trivial solutions (38) and (39) and the first boundary condition of (30):

$$\hat{f}_{\mathrm{down}}(\hat{r},\,\hat{l}-0) = \begin{cases} 1 & \text{for } 0 \leqslant \hat{r} \leqslant 1, \\ 0 & \text{for } \hat{r} > 1. \end{cases} \tag{42}$$

Substituting this boundary value at $\hat{\zeta}_{\mathrm{top}} = \hat{l} - 0$ into (37), we obtain the following:

$$\hat{f}_{\mathrm{down}}(\hat{r},\,\hat{z}) = -\frac{1}{2(\hat{z}-\hat{l})}\int_0^1 I_0\left(-\frac{\hat{r}\hat{\rho}}{2(\hat{z}-\hat{l})}\right)\exp\left(\frac{\hat{r}^2+\hat{\rho}^2}{4(\hat{z}-\hat{l})}\right)\hat{\rho}\;\mathrm{d}\hat{\rho}$$
$$\text{in domain } 2(\hat{z} < \hat{l}). \tag{43}$$

Figure 6(a) shows $\hat{u}_z$ around the rising particle given by the above $\hat{f}_{\mathrm{up}}$ and $\hat{f}_{\mathrm{down}}$ where the integral in (41) and (43) are obtained by numerical integration. The flow velocity obtained using (36) and (37) is identical to the Fourier–Bessel transform solution of Chang (1963) and the a superposition of MHD Oseenlet of Ueno and Yasuda (2003).

The drag of the rising particle is given by the pressure difference between the upper surface $\hat{z} = \hat{l} + 0$ and the lower surface $\hat{z} = \hat{l} - 0$ of the particle:

$$\hat{D} = 2\pi\int_0^1 \hat{p}(\hat{r},\,\hat{l}+0)\;\hat{r}\;\mathrm{d}\hat{r} - 2\pi\int_0^1 \hat{p}(\hat{r},\,\hat{l}-0)\;\hat{r}\;\mathrm{d}\hat{r}$$
$$= 2\pi\int_0^1 \{\hat{f}_{\mathrm{up}}(\hat{r},\,\hat{l}+0) - \hat{f}_{\mathrm{down}}(\hat{r},\,\hat{l}+0) - \hat{f}_{\mathrm{up}}(\hat{r},\,\hat{l}-0) + \hat{f}_{\mathrm{down}}(\hat{r},\,\hat{l}-0)\}\;\hat{r}\;\mathrm{d}\hat{r}. \tag{44}$$

By substituting the lower boundary values (38) and (40) of domain 1 and the upper boundary values (39) and (42) of domain 2, we obtain the following:

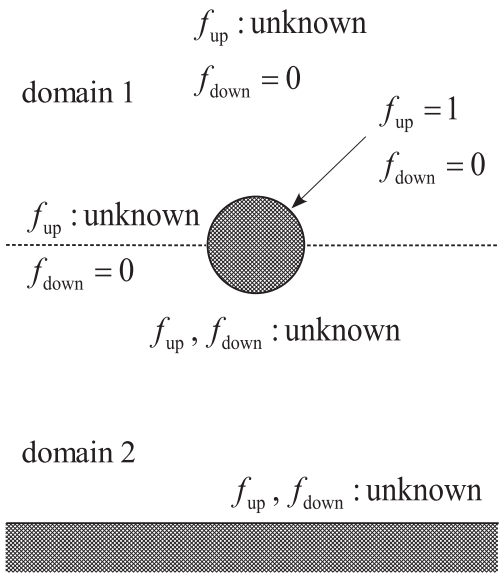

Figure 4. Division of the space in the case considering the vessel bottom wall.

$$\hat{D} = 2\pi. \tag{45}$$

The result obtained by converting this dimensionless value into a dimensional value is identical to the Chester's drag law $D_{\text{chester}} = 2\pi(\sigma\eta)^{1/2}a^2U_0B_0$. Thus, formulas (36) and (37) are verified.

5. Effect of vessel bottom wall

Let us consider the flow field and drag when affected by the vessel bottom wall. The boundary values are unknown variables because the particle surface and vessel bottom wall influence each other.

5.1. Numerical solutions obtained by the boundary element method

Numerical solutions of the boundary values were obtained by the boundary element method. We divided the space into two domains as shown in figure 4. The Green function method was applied for each domain.

We divided the bottom of domain 2 into boundary elements, where discretized variables are denoted by $(\hat{f}_{\text{up}}^{\text{btm}})_{ib}$ and $(\hat{f}_{\text{down}}^{\text{btm}})_{ib}$. In addition, we divided the lower surface of the particle into boundary elements, where discretized variables are denoted by $(\hat{f}_{\text{up}}^{\text{ptc}})_{ip}$ and $(\hat{f}_{\text{down}}^{\text{ptc}})_{ip}$. Furthermore, we divided a fluid part of the boundary of domain 1 and domain 2, except the particle ($\hat{r} > 1$), into boundary elements, where discretized variables are denoted by $(\hat{f}_{\text{up}}^{\text{top}})_{it}$ and $(\hat{f}_{\text{down}}^{\text{top}})_{it}$. Subscripts *ib*, *ip*, and *it* indicate the element numbers of the bottom boundary, lower surface of particle $\hat{r} < 1$, and fluid boundary $\hat{r} > 1$, respectively. Subscripts *jb*, *jp*, *jt* or *kb*, *kp*, and *kt* are used if necessary.

Let us consider $\hat{f}_{\text{up}}(\hat{r}, \hat{z})$ in (36) when $(\hat{r}, \hat{z})$ is the center of a boundary element at the top boundary of domain 2. In addition, we consider $\hat{f}_{\text{down}}(\hat{r}, \hat{z})$ in (37) when $(\hat{r}, \hat{z})$ is the center of

a boundary element at the bottom boundary of domain 2. The right side of (36) is integrated for the bottom boundary, and the right side of (37) is integrated for the top boundary. These are simultaneous integral equations for boundary values. Integration of both equations are approximated by the numerical integral of each boundary element, and therefore, we obtain relationship (46) with respect to discretized boundary values.

$$
\begin{aligned}
(\hat{f}^{\mathrm{ptc}}_{\mathrm{up}})_{ip} &= \sum_{jb} A_{ip,jb}\ (\hat{f}^{\mathrm{btm}}_{\mathrm{up}})_{jb},\\
(\hat{f}^{\mathrm{top}}_{\mathrm{up}})_{it} &= \sum_{jb} A^{*}_{it,jb}\ (\hat{f}^{\mathrm{btm}}_{\mathrm{up}})_{jb},\\
(\hat{f}^{\mathrm{btm}}_{\mathrm{down}})_{ib} &= \sum_{jp} B_{ib,jp}\ (\hat{f}^{\mathrm{ptc}}_{\mathrm{down}})_{jp} + \sum_{jt} B^{*}_{ib,jt}\ (\hat{f}^{\mathrm{top}}_{\mathrm{down}})_{jt}.
\end{aligned}
\tag{46}
$$

The boundary element in this study are 0th order elements. The unknown variable is constant in each element. The coefficient matrix is given by the integral kernel. We execute the numerical integral by the Gauss integral method for the boundary element.

Boundary conditions (30) give the following:

$$
\begin{aligned}
(\hat{f}^{\mathrm{ptc}}_{\mathrm{up}})_{ip} + (\hat{f}^{\mathrm{ptc}}_{\mathrm{down}})_{ip} &= 1,\\
(\hat{f}^{\mathrm{btm}}_{\mathrm{up}})_{ib} + (\hat{f}^{\mathrm{btm}}_{\mathrm{down}})_{ib} &= 0.
\end{aligned}
\tag{47}
$$

Further, a continuity between domain 1 and domain 2 gives the following:

$$
(\hat{f}^{\mathrm{top}}_{\mathrm{down}})_{it} = 0. \tag{48}
$$

Here, the trivial solution $\hat{f}_{\mathrm{down}}(\hat{r}, \hat{z}) = 0$ is considered in domain 1.

Boundary element equations (46)–(48) are reduced as follows:

$$
\sum_{kp}\left(\delta_{ip,kp} - \sum_{jb} A_{ip,jb}\ B_{jb,kp}\right)(\hat{f}^{\mathrm{ptc}}_{\mathrm{down}})_{kp} = 1. \tag{49}
$$

The coefficient matrix of these simultaneous linear equations is a full matrix. Those matrices are solved by LU decomposition, and $(\hat{f}^{\mathrm{ptc}}_{\mathrm{down}})_{kp}$ is determined.

After a numerical solution of $(\hat{f}^{\mathrm{ptc}}_{\mathrm{down}})_{kp}$ is obtained, we obtain the other boundary value by substituting $(\hat{f}^{\mathrm{ptc}}_{\mathrm{down}})_{kp}$ into the following formulas.

$$
\begin{aligned}
(\hat{f}^{\mathrm{ptc}}_{\mathrm{up}})_{ip} &= 1 - (\hat{f}^{\mathrm{ptc}}_{\mathrm{down}})_{ip},\\
(\hat{f}^{\mathrm{btm}}_{\mathrm{down}})_{ib} &= \sum_{jp} B_{ib,jp}\ (\hat{f}^{\mathrm{ptc}}_{\mathrm{down}})_{jp},\\
(\hat{f}^{\mathrm{btm}}_{\mathrm{up}})_{ib} &= -(\hat{f}^{\mathrm{btm}}_{\mathrm{down}})_{ib},\\
(\hat{f}^{\mathrm{top}}_{\mathrm{up}})_{it} &= \sum_{jb} A^{*}_{it,jb}\ (\hat{f}^{\mathrm{btm}}_{\mathrm{up}})_{jb}.
\end{aligned}
\tag{50}
$$

When all numerical solutions of the boundary elements in domain 2 are obtained, we can find the solution of the arbitrary point in domain 2 by substituting the numerical solution into (36) and (37). This procedure does not involve integral equations but straightforward numerical integrations.

We obtained only $\hat{f}_{\mathrm{up}}(\hat{r}, \hat{z})$ because $\hat{f}_{\mathrm{down}}(\hat{r}, \hat{z})$ is $\hat{f}_{\mathrm{down}}(\hat{r}, \hat{z}) = 0$ in domain 1. The boundary value of the bottom of domain 1 is given as follows:

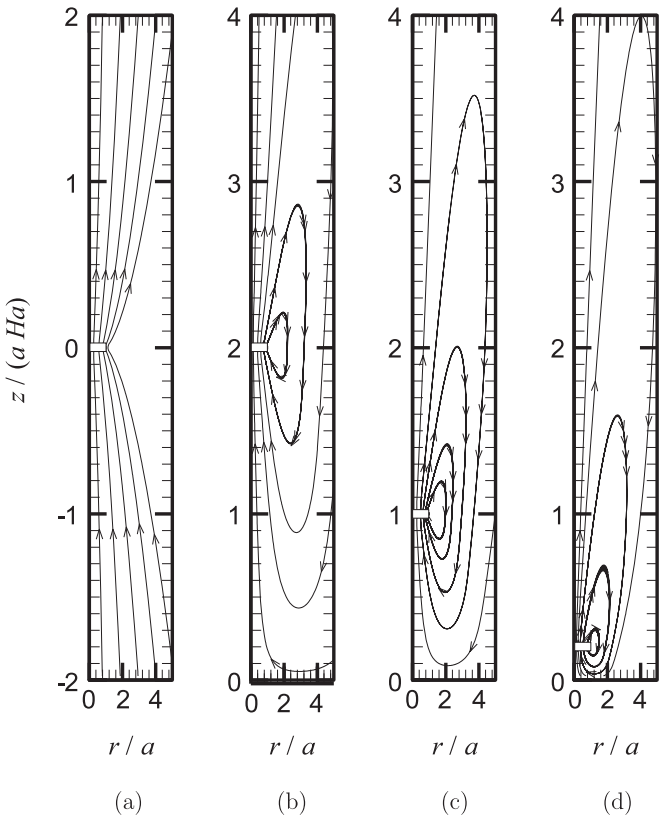

Figure 5. Stream lines; (a) free space, (b) $l = 2.0aHa$, (c) $l = 1.0aHa$, (d) $l = 0.2aHa$. These four cases do not show time development but independent cases to each other.

$$\hat{f}_{\mathrm{up}}(\hat{\rho}, \hat{\zeta}_{\mathrm{btm}}) = \begin{cases} 1 & \text{for} 0 \leqslant \hat{\rho} < 1, \\ (\hat{f}_{\mathrm{up}}^{\mathrm{top}})_{it} & \text{for} \hat{\rho} > 1. \end{cases} \tag{51}$$

The continuity between solution $(\hat{f}_{\mathrm{up}}^{\mathrm{top}})_{it}$ of domain 2 and $\hat{f}_{\mathrm{up}}(\hat{\rho}, \hat{\zeta}_{\mathrm{btm}})$ of domain 1 is required for $\hat{\rho} > 1$. By substituting (51) into (36), we obtained the solution of arbitrary point in domain 1.

The flow fields for various distances $\hat{l}$ between a rising particle and vessel bottom wall were calculated. Figure 5 shows the stream lines. The vessel bottom wall is located at $z = 0$ in (b)–(d). These cases shown in figure 5 do not show time development, but show independent cases. The result of this problem is a dynamically similar solution for $Ha \gg 1$, where we use the compressed coordinates (12). The actual flow field for an arbitrary value of Ha is derived by multiplying appropriate similarity ratio with the similar solution. The aspect ratio in figures 5–7 is magnified ten times in the vertical direction. This aspect ratio corresponds to the flow field for $Ha = 10$.

Figure 6 shows the distributions of the velocity component in the vertical direction. Fluid rises with the rising particle within the distance $|z - l| \lesssim 0.1aHa$ from the particle. In the absence of the vessel bottom wall, the fluid in the side region $r > a$ of the particle is stationary. On the other hand, when the vessel bottom wall exists, a downward flow is

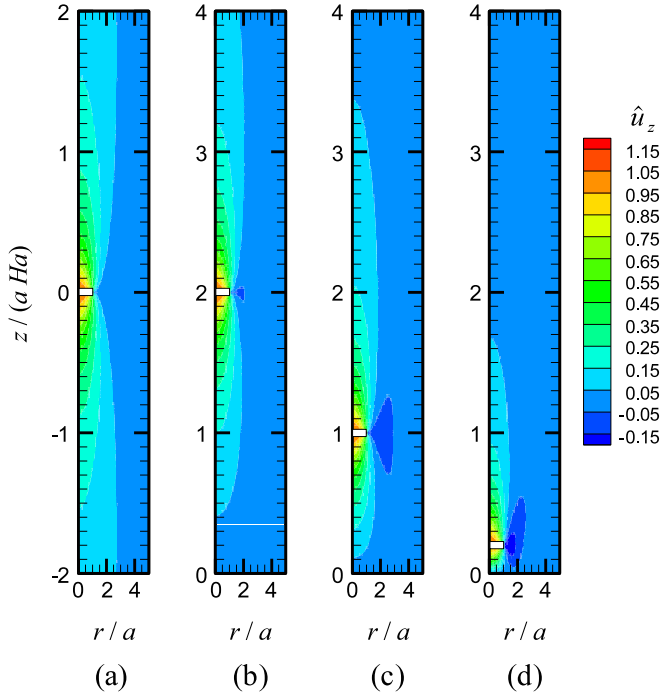

Figure 6. Distributions of vertical component $\hat{u}_z$ of the velocity; (a) free space, (b) $\hat{l} = 2.0$, (c) $\hat{l} = 1.0$, (d) $\hat{l} = 0.2$.

generated in the side region of the particle. This downward velocity remarkably increases when the distance between particle and the vessel bottom wall decreases.

The extent of flow in the side region of the rising particle is several times the particle radius regardless of whether the vessel bottom wall affects the flow. Hence, analysis of this study is applicable to the flows in vessel except the flow induced by a rising particle in the vicinity of the side walls. In other words, the effects of the side walls are confined to their vicinity.

Figure 7 show the distribution of pressure. The pressure is high above the particle and low below the particle. Therefore, a downward force is generated. The pressure at the bottom of a particle decreases when the distance between the particle and the vessel bottom wall decreases.

Figure 8 show the relation between the particle position and drag. Drag asymptotically converges with Chester's drag when the distance between the particle and the vessel bottom wall increases. On the other hand, the drag remarkably increases when the distance between the particle and vessel wall decreases. The relation between particle position and drag is discussed further in the next section.

5.2. Analytic approach to drag law

In the preceding section, we numerically obtained the drag when the vessel bottom wall existed. In this section, we derive an approximate evaluation by an analytic approach for $\hat{l} \gg 1$. The solution in domain 2 is obtained by successive approximation. Here, (39) and (43) are adopted as the first approximations of the solution in domain 2:

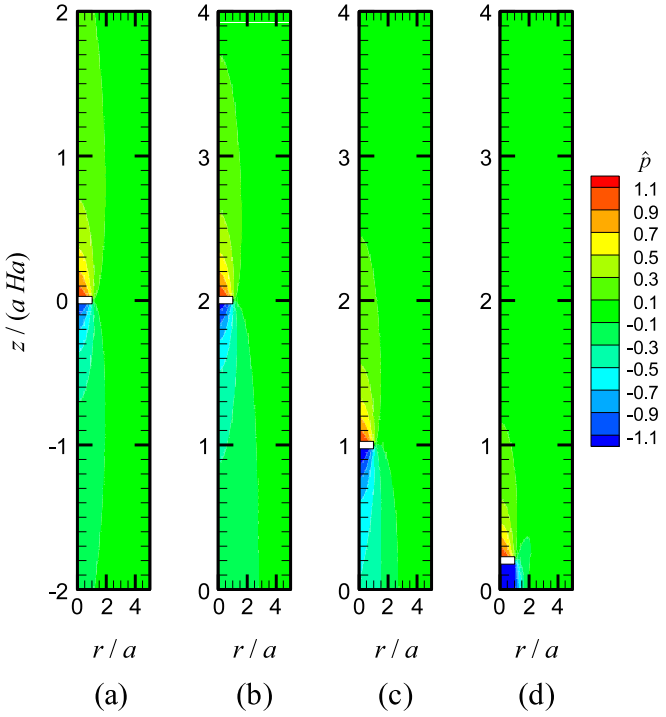

Figure 7. Distribution of the pressure $\hat{p}$; (a) free space, (b) $\hat{l} = 2.0$, (c) $\hat{l} = 1.0$, (d) $\hat{l} = 0.2$.

$$\hat{f}_{\mathrm{up}}^{(0)}(\hat{r}, \hat{z}) = 0,$$

$$\hat{f}_{\mathrm{down}}^{(0)}(\hat{r}, \hat{z}) = -\frac{1}{2(\hat{z} - \hat{l})} \int_0^1 I_0\left(-\frac{\hat{r}\hat{\rho}}{2(\hat{z} - \hat{l})}\right) \exp\left(\frac{\hat{r}^2 + \hat{\rho}^2}{4(\hat{z} - \hat{l})}\right) \hat{\rho}\, \mathrm{d}\hat{\rho}. \tag{52}$$

Equation (52) does not satisfy the boundary condition for the vessel bottom wall. Hence, it is corrected for satisfying $\hat{f}_{\mathrm{up}} + \hat{f}_{\mathrm{down}} = 0$.

$$\hat{f}_{\mathrm{up}}^{(1)}(\hat{r}, 0) = -\frac{1}{2\hat{l}} \int_0^1 I_0\left(\frac{\hat{r}\hat{\rho}}{2\hat{l}}\right) \exp\left(-\frac{\hat{r}^2 + \hat{\rho}^2}{4\hat{l}}\right) \hat{\rho}\, \mathrm{d}\hat{\rho}. \tag{53}$$

The function $\hat{f}_{\mathrm{up}}^{(1)}(\hat{r}, \hat{z})$ is obtained in the whole domain 2 by substituting (53) into the integration of right-hand side of (36). The following integral gives $\hat{f}_{\mathrm{up}}^{(1)}$ at the lower surface of the particle:

$$\hat{f}_{\mathrm{up}}^{(1)}(\hat{r}, \hat{l} - 0) = -\frac{1}{4\hat{l}^2} \int_0^\infty \int_0^1 I_0\left(\frac{\hat{r}\hat{s}}{2\hat{l}}\right) I_0\left(\frac{\hat{s}\hat{\rho}}{2\hat{l}}\right) \exp\left(-\frac{\hat{r}^2 + 2\hat{s}^2 + \hat{\rho}^2}{4\hat{l}}\right) \hat{\rho}\hat{s}\, \mathrm{d}\hat{\rho}\, \mathrm{d}\hat{s}. \tag{54}$$

The boundary condition in the lower surface of the particle is not satisfied by using $\hat{f}_{\mathrm{up}}^{(1)}$. Hence, $\hat{f}_{\mathrm{down}}$ is corrected to satisfy $\hat{f}_{\mathrm{up}} + \hat{f}_{\mathrm{down}} = 1$ ($\hat{r} < 1$):

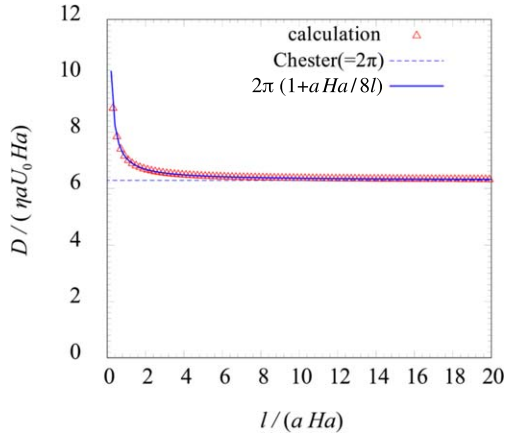

Figure 8. The relation between dimensionless particle position $\hat{l} = l/(a\ Ha)$ and dimensionless drag $\hat{D} = D/(\eta a U_0 Ha)$.

$$\hat{f}^{(1)}_{\mathrm{down}}(\hat{r},\ \hat{l}\ -\ 0) = \begin{cases} 1 + \dfrac{1}{4\hat{l}^2}\displaystyle\int_0^{\infty}\int_0^{1} I_0\left(\frac{\hat{r}\hat{s}}{2\hat{l}}\right) I_0\left(\frac{\hat{s}\hat{\rho}}{2\hat{l}}\right) \exp\left(-\frac{\hat{r}^2 + 2\hat{s}^2 + \hat{\rho}^2}{4\hat{l}}\right)\hat{\rho}\hat{s}\ \mathrm{d}\hat{\rho}\ \mathrm{d}\hat{s} \\ \qquad\qquad \text{for } 0 \leqslant \hat{r} \leqslant 1, \\ 0 \qquad\qquad \text{for } \hat{r} > 1. \end{cases} \tag{55}$$

By substituting (55) into the right side of (37), $\hat{f}^{(1)}_{\mathrm{down}}(\hat{r},\ \hat{z})$ in the whole domain 2 is obtained.

The functions $\hat{f}^{(1)}_{\mathrm{up}}$ and $\hat{f}^{(1)}_{\mathrm{down}}$ do not satisfy the boundary condition for the vessel bottom wall. Therefore, we correct $\hat{f}_{\mathrm{up}}$ again as $\hat{f}^{(2)}_{\mathrm{up}}$. By repeating this process, the correction term $O(\hat{l}^{-2n})$ is added to each repetition of n. The precision in the first correction is sufficient when $\hat{l} \gg 1$. Therefore, $\hat{f}^{(1)}_{\mathrm{up}}$ and $\hat{f}^{(1)}_{\mathrm{down}}$ are used in this paper.

By using this approximation, the pressure of the lower surface of the particle is given as follows:

$$\begin{aligned} p^{(1)}(\hat{r},\ \hat{l}\ -\ 0) &= \hat{f}^{(1)}_{\mathrm{up}}(\hat{r},\ \hat{l}\ -\ 0) - \hat{f}^{(1)}_{\mathrm{down}}(\hat{r},\ \hat{l}\ -\ 0) \\ &= -1 - \frac{1}{2\hat{l}^2}\int_0^{\infty}\int_0^{1} I_0\left(\frac{\hat{r}\hat{s}}{2\hat{l}}\right) I_0\left(\frac{\hat{s}\hat{\rho}}{2\hat{l}}\right) \exp\left(-\frac{\hat{r}^2 + 2\hat{s}^2 + \hat{\rho}^2}{4\hat{l}}\right)\hat{\rho}\hat{s}\ \mathrm{d}\hat{\rho}\ \mathrm{d}\hat{s} \\ &\quad \text{for } 0 \leqslant \hat{r} \leqslant 1. \end{aligned} \tag{56}$$

On the other hand, the pressure of the upper surface of the particle is given by $\hat{f}^{(1)}_{\mathrm{up}}(\hat{r},\ \hat{l}\ +\ 0) = 1$ and $\hat{f}^{(1)}_{\mathrm{down}}(\hat{r},\ \hat{l}\ +\ 0) = 0$:

$$p^{(1)}(\hat{r},\ \hat{l}\ +\ 0) = 1. \tag{57}$$

The drag of the particle is found by subtracting the pressure of the lower surface of the particle from that of the upper surface of the particle:

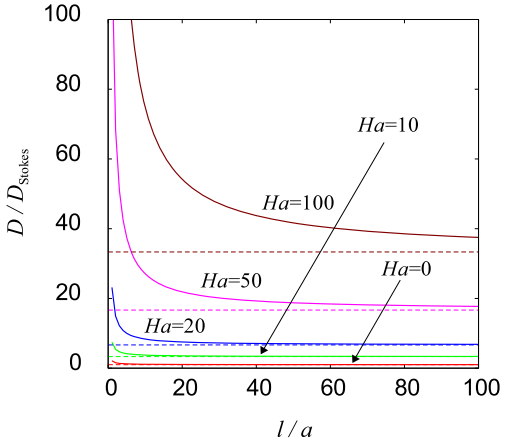

Figure 9. The relation between particle position l and drag D for various Hartmann number; ——: drag affected by the vessel bottom wall, - - - -: drag in free space.

$$\hat{D} = 2\pi \int_0^1 p^{(1)}(\hat{r}, \hat{l} + 0)\hat{r}\, d\hat{r} - 2\pi \int_0^1 p^{(1)}(\hat{r}, \hat{l} - 0)\hat{r}\, d\hat{r}$$
$$= 2\pi + \frac{\pi}{\hat{l}^2} \int_0^1 \int_0^\infty \int_0^1 I_0\left(\frac{\hat{r}\hat{s}}{2\hat{l}}\right) I_0\left(\frac{\hat{s}\hat{\rho}}{2\hat{l}}\right) \exp\left(-\frac{\hat{r}^2 + 2\hat{s}^2 + \hat{\rho}^2}{4\hat{l}}\right) \hat{\rho}\hat{s}\hat{r}\, \mathrm{d}\hat{\rho}\, \mathrm{d}\hat{s}\, \mathrm{d}\hat{r}. \tag{58}$$

The triple integral of (58) is approximated by $\hat{l}/4$ for $\hat{l} \gg 1$.

$$\hat{D} = 2\pi\left(1 + \frac{1}{8\hat{l}}\right). \tag{59}$$

The first term in the parenthesis shows Chester's drag in free space, and the second term shows a correction with respect to the vessel bottom wall. Figure 8 shows this result using a solid line. The analytic result agrees well with the result by the boundary element method for $\hat{l} > 1$. The increment of drag when the vessel bottom wall exists is inversely proportional to the distance between the particle and vessel bottom wall.

We rewrite (59) in a dimensional form:

$$D = 2\pi\eta a U_0 Ha\left(1 + \frac{a}{8l} Ha\right) = 2\pi\sqrt{\sigma\eta}\; a^2 U_0 B_0\left(1 + \sqrt{\frac{\sigma}{\eta}}\frac{a^2 B_0}{8l}\right). \tag{60}$$

The vertical axis in figure 9 shows the ratio of the obtained drag D to Stokes's drag D_{stokes} of a particle in free space.

$$\frac{D}{D_{\mathrm{stokes}}} = \frac{Ha}{3}\left(1 + \frac{a}{8l} Ha\right). \tag{61}$$

The solid line for $Ha = 0$ in figure 9 shows the ratio of Stokes's drag in the presence of the vessel bottom wall (Brenner 1962, Happel and Brenner 1965) and D_{stokes}. The horizontal axis shows the ratio of the distance between the particle and vessel bottom wall and particle radius l/a. Correction terms for both non-conducting and conducting fluids are proportional to a/l. Nevertheless, the origins of these corrections are different: viscous force causes the correction in non-conducting fluids while electromagnetic force causes the correction in conducting fluids. The drag remarkably increases when Ha increases. Moreover, the region of influence of the vessel bottom wall expands with Ha. The influence of the vessel bottom wall is not

localized in the neighborhood of the bottom wall but spreads over a large region along the magnetic flux lines. Therefore, Chester's drag in free space is insufficient for representing the drag of particle in a vessel under a strong magnetic field.

6. Conclusion

We studied a particle rising along a vertical magnetic field in an electrically conducting fluid. We obtained the fluid flow around the particle and the drag of the particle in the presence of the vessel bottom. A system of simplified differential equations of the flow field using compressed coordinates were derived when the Hartmann number Ha was much larger than one, Reynolds number was much smaller than the Hartmann number, and the magnetic Reynolds number was much smaller than one. The solution of this system of equations represents a dynamically similar flow that is characterized by the dimensionless distance $\hat{l} = l/(a\ Ha)$ between the particle and the vessel bottom wall. Anisotropy of the flow field is included not in the similar solution but in the coordinate compression. The flow field is obtained in form of the superposition of the upward spatial-evolution function and downward spatial-evolution function along the magnetic flux line. The drag of the rising particle $D = 2\pi\eta a U_0 Ha\{1 + (a/8l)Ha\}$ considering the influence of the vessel bottom wall is obtained. The first term in the parenthesis shows Chester's drag in free space, and the second term shows a correction with respect to the vessel bottom wall. The drag remarkably increases when the distance l between the particle and vessel bottom decreases. The influence region $a\ Ha$ of the vessel bottom wall expands along the magnetic flux lines when the Hartmann number increases. Therefore, the correction term of drag affects a large region in the vessel when the magnetic field is very strong. On the other hand, the extent of the flow in the side region of the rising particle is several times the particle radius a regardless of the effect of the vessel bottom wall on the flow. Hence, the effects of the side walls are confined in the vicinity of these walls.

References

Brenner H 1962 Effect of finite boundaries on the Stokes resistance of an arbitrary particle *J. Fluid Mech.* **12** 35–48

Chang I D 1963 On a singular perturbation problem in magnetohydrodynamics *ZAMP* **14** 134–47

Chester W 1961 The effect of a magnetic field on the flow of a conducting fluid past a body of revolution *J. Fluid Mech.* **10** 459–65

Chester W and Moore D W 1961 The effect of a magnetic field on the flow of a conducting fluid past a circular disk *J. Fluid Mech.* **10** 466–72

Happel J and Brenner H 1965 *Low Reynolds Number Hydrodynamics* (Englewood Cliffs, NJ: Prentice-Hall) p 87

Kyrlidis A, Brown R A and Walker J S 1990 Creeping flow of a conducting fluid past axisymmetric bodies in the presence of an aligned magnetic field *Phys. Fluids* A **2** 2230–9

Ueno K and Yasuda H 2003 MHD oseenlet and double wake of a rising sphere under a strong vertical magnetic field *Magnetohydrodynamics* **39** 547–55

Wrobel L C 2002 *The Boundary Element Method* vol 1 (New York: Wiley)

Yasuda H, Ohnaka I, Kawakami O, Yamamoto M, Ueno K and Kishio K 2001 Effect of a high magnetic field on monotectic solidification *4th Pacific Rim Int. Conf. Adv. Mater. and Processing* (Japan Institute of Metals) pp 289–92

Yasuda H, Ohnaka I, Kawakami O, Ueno K and Kishio K 2003 Effect of magnetic field on solidification in Cu-Pb monotectic alloys *ISIJ Int. J.* **43** 942–9